Title: What is the Probability of Induced Seismicity Triggering a Major Earthquake in the Salton Sea?

EMILY E. BRODSKY
DEPT. OF EARTH & PLANETARY SCIENCES, UNIVERSITY OF CALIFORNIA, SANTA CRUZ

Geothermal power generation commonly induces seismicity. We have shown that the earthquakes in the Salton Sea region are directly related to the net extraction of fluid in the field. We used an ETAS model to decluster the catalog and then related the background rate to publically available monthly injection and production data. The success of this project also shows that the induced earthquakes have aftershocks, which can potentially occur on other faults in the region. Therefore, it is possible that induced seismicity can trigger tectonic events. This project specifically addresses SCEC4 problem 2f focusing on induced seismicity in the Salton Sea area.

The exploitation of geothermal resources is rapidly expanding as society increases its reliance on renewable energy sources. Production of geothermal power induces seismicity as water is pumped both into and out of a reservoir (Majer et al., 2007; Nicol et al., 2011). Fluid injection, a major component of most geothermal operations, has been shown to induce seismicity in a variety of settings and the earthquakes are often attributed to a decrease in the effective stress on faults due to increased pore pressure (Evans et al., 2012; Frohlich et al., 2011; Keranen et al., 2013; Nicholson and Wesson, 1992; Raleigh et al., 1976). Earthquakes can also be induced by fluid extraction through more complex processes such as thermal contraction or subsidence-driven increases in shear stress (McGarr et al., 2002; Mossop and Segall, 1999). Seismic consequences of geothermal production are of particular concern for facilities neighboring large tectonic systems. Therefore, it is important to understand the controls on geothermal production-related seismicity in a setting like the Salton Sea Geothermal Field, which borders the diffuse terminus of the San Andreas Fault system in southern California.

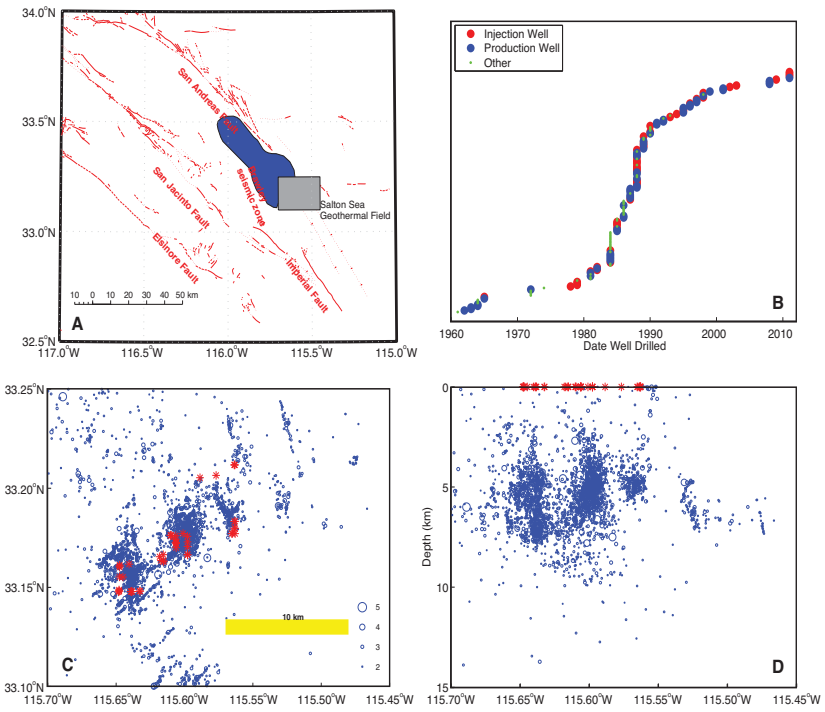

Figure 1. Earthquake and geothermal facility locations and activity. (A) Regional map with faults and location of the Salton Sea Geothermal Field. **(B)** Drill year of the wells in the field for 1960-2012. **(C)** Earthquakes (blue circles) and injection wells (red stars) in map view. **(D)** E-W cross-sectional view. Earthquake hypocenters cluster around and beneath injection wells. Depth is relatively poorly constrained in the sedimentary basin (Chu and Helmberger, 2013) and is not used for any subsequent statistics in this study.

The Salton Trough is home to four operating geothermal fields (Salton Sea, Brawley, Heber, and East Mesa) that generate a total of over 650 MW of electricity (Fig. 1). The Salton Sea Geothermal Field exploits a hot, geothermal brine with temperatures in excess of 320° C at 2 km depth (Muffler and White, 1969; Younker et al., 1982). The field includes ten operating geothermal power plants with a total capacity of approximately 330 MW. Plants use flash technologies that extract fluid from depth and flash a portion to steam to power generators, while the remaining brine is either injected via separate wells back into the reservoir, or subjected to further flashing. Steam condensate is also recaptured for injection. The volume of fluid loss during operations depends on a variety of conditions including salinity in the flashing chambers and air temperature. Since 1992, the average reported monthly injection volume is 81% of the reported production volume with a standard deviation of 7%. Production at the plant cycles annually in response to demand and local environmental conditions.

The first plant came online at the Salton Sea Geothermal Field in 1982. Operations expanded steadily from 1991 with new wells regularly added and fluid volumes increasing through 2005 (Fig. 1B; Fig. 2). For the highest production month in 2012, 11.2 x 10^9 kg (~10^7 cubic meters) of geothermal fluid was extracted from the reservoir at depths of ~1 to 2.5 km, and 9.2 x 10^9 kg was injected at similar depths.

We quantified the relationship between fluid volumes within the Salton Sea Geothermal Field and the local rate of seismicity by combining publically available datasets. By law, in California the monthly field-wide total production and injection volumes are released to the California Department of Conservation. For earthquake locations and times, we used the largest high precision catalog available for the region (Hauksson et al., 2012) for January 1981- June 2011 supplemented by the Southern California Seismic Network catalog for July 2011-December 2012. Station configurations have changed over time with a notable increase in data after the release of the geothermal field's local seismic network in 2007. Therefore, we restrict the data to the local magnitude of completeness of 1.75 to ensure that we only analyze events that are large enough to have been detectable throughout the study period. For this study, the Salton Sea Geothermal Field seismicity is defined as earthquakes shallower than 15 km in the region bounded by 33.1-33.25^o N and 115.7-115.45^o W (Fig. 1).

The seismicity rate has mirrored overall activity in the field (Fig 1). As noted by earlier, earthquakes clusters around injection wells both at the surface and at depth (Chen and Shearer, 2011),. The seismicity rate was initially low during the period of low-level geothermal operations before 1986. As operations expanded, so did the seismicity. The maximum net volume production rate occurred in July 2005, which is a month before the largest earthquake rate increase. This August 2005 swarm has been linked to a creep transient, but had not been compared previously to the production data (Llenos et al., 2009; Lohman and McGuire, 2007).

However, the relationship between seismicity and plant operations is not simple. Earthquakes are highly clustered due to local aftershock sequences and so it is difficult to untangle the direct influence of human activities from secondary earthquake triggering. In addition, seismicity rate varies over orders of magnitude, whereas pumping conditions evolve more smoothly. Operations are continually changing at the plants in response to both economic and natural factors. These issues complicate the data so that a simple correlation between the raw seismicity rate and operational parameters is suggested, but unclear and requires further analysis.

Because earthquakes commonly have aftershocks, any statistical method that assumes independence of events is problematic. A better approach is to measure the background rate over time, separate from the secondary triggering of aftershocks. In this context the term "background rate" means the primary earthquakes directly related to the driving stress from both tectonic and anthropogenic sources, and therefore the background rate can vary in time.

To separate background and aftershock seismicity, we used the Epidemic Type Aftershock Sequence (ETAS) model in which background and aftershock rates are parameterized using standard empirical relationships and the resulting parameter set is simultaneously fit from the observed catalog (Ogata, 1992). This strategy builds on previous work on identifying fluid-modulated signals in natural and induced seismicity (Bachmann et al., 2011; Hainzl and Ogata, 2005; Lei et al., 2008; Ogata, 1992). The seismicity is modeled as a Poissonian process with history-dependent rate R_{ETAS} at time t_E that is a

combination of the modified Omori's law, which describes the temporal decay of aftershocks, the Gutenberg-Richter relationship, which describes the magnitude distribution, and the aftershock productivity relationship, i.e.,

$$R_{ETAS}(t_E) = \mu + \sum_{i;t_i<t_E} \frac{K_E 10^{\alpha(M_i - M_c)}}{(t_E - t_i + c)^p} \quad (1)$$

where μ is background seismicity rate and the term inside the summation describes the component of seismicity due to aftershock sequences. In this formulation, K_E is the aftershock productivity of a mainshock, α describes the efficiency of earthquakes of a given magnitude at generating aftershocks, c and p are Omori's law decay parameters, M_i and t_i are the magnitude and time of the i^{th} event in the catalog, and M_c is the magnitude completeness threshold of the catalog (Brodsky, 2011; Ogata, 1992).

We perform maximum likelihood fits on overlapping two-year windows and track background seismicity rate over time (Fig. 2). We assume that the background rate is stationary for relatively short times, i.e., over the two-year interval, but varies over the long duration of the full catalog. The two-year interval allows sufficient events to have well-resolved parameters, while still capturing the high-frequency fluctuations.

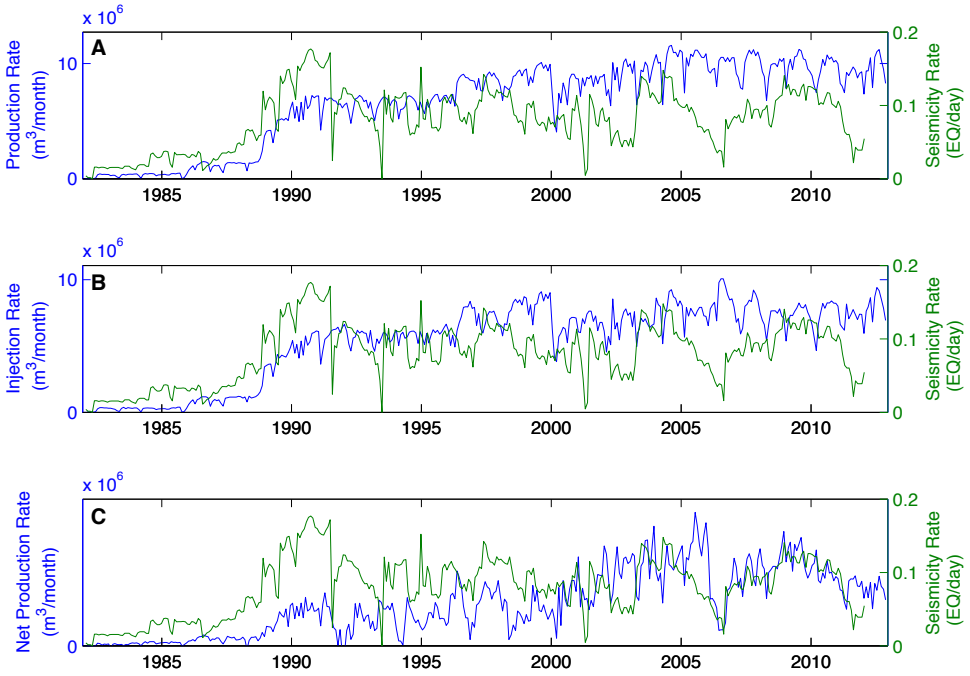

Figure 2. Background seismicity rate (μ) over time compared to operational fluid volumes at the Salton Sea Geothermal Field. The seismicity rate curve is identical for each panel (right hand axis, green curve) and the operational rate (left axis, blue curve) in each case is **(A)** Production rate, **(B)** Injection rate and **(C)** Net Production rate. Seismicity rate estimation is on 2-year overlapping intervals centered on each month for which there is operational data.

The increasing trend of the background rate μ in Fig. 2 imitates all the metrics of fluid volume (injection, production, and net production, defined here as production minus injection), particularly in the earlier years of injection (until ~1991). In later years (2006 to 2012), μ tracks net production more closely. In between, seismicity may track net production with a baseline shift (Fig. 2c), but the correlations are much less clear. Both total and net production seem important.

The time variable behavior is captured by the best-fit coefficients of a linear model, i.e,

$$\mu = c_1 I + c_2 N \quad (2)$$

where I and N are the injection and net production rate, respectively, and c_1 and c_2 are the coefficients. Because the correlation between total injection and total production is extremely high, only one of those variables is used in Eq. 2 to ensure a well-constrained solution. We measure time-variation by fitting Eq. 2 over a moving data window that is longer in duration than the window used to fit the ETAS model and much shorter than the full study interval. A linear least-squares fit in a 6-year window with 0.5 year increments (i.e., ~90% overlap) captures the essential features (Fig. 3).

The combined model of Eq. 2 results in well-constrained model parameters after the initial growth of operations in the mid-1980's. An F-test rejects the null hypothesis of insignificant fit at the 95% level for all time periods except during the rapid growth of the field in 1993. The early years have substantial uncertainty in the fit coefficients, as might be expected during the highly non-steady initial phase of operations. During the well-fit period, the seismicity rate generated per monthly volume of fluid injected steadily decreases over time. Net production generates more earthquakes per fluid volume than injection both early and late in the study period.

In addition to the difference in correlations over time, there is a difference in phase lags between seismicity and the various operational parameters. The phase lag corresponding to the maximum correlation of seismicity relative to net production is usually 0 months. However, the intervals with the strongest correlations between injection or production and seismicity can have several month phase lags. Over the full dataset, the maximum correlation between seismicity and injection has a lag of 8 months. In intervals like 1991-2006, unphysical, large phase lags accompany low correlations and are another indicator of the lack of predictive power of a single operational parameter during these periods.

We conclude from the observed correlations and the F-test that net production volume combined with injection information is a good predictor of the seismic response in the short term for a fully developed field. Much previous work (Evans et al., 2012; Frohlich et al., 2011; Keranen et al., 2013; Raleigh et al., 1976; Shapiro et al., 2010) has focused on the increase in pore pressure (decrease in effective stress) from injection as the primary driver of seismicity, and the importance of net production (volume removed) suggests that seismicity is responding to a more complex process. Earthquakes responding to net volume loss with no phase lag may imply that seismicity responds to elastic compaction and subsidence, and not simply diffusion of high pore pressures at injection sites (McGarr et al., 2002; Mossop and Segall, 1999).

An important issue for any induced seismicity study is the possibility of triggering a damaging earthquake. Like most earthquake sequences, the Salton Sea Geothermal Field seismicity is dominated by small earthquakes and the magnitude distribution follows the Gutenberg-Richter relationship, i.e., the number of earthquakes of magnitude greater than or equal to M is proportional to 10^{-bM} where b is nearly 1 (The maximum likelihood estimate of b for 1982-2012 is 0.99). Static and dynamic stresses have been observed to trigger earthquakes on disconnected fault networks (King et al., 1994; van der Elst and Brodsky, 2010) and the Gutenberg-Richter relationship generally holds for the aggregated sequences (Ogata, 1992; Woessner et al., 2011). The major limitation in applying Gutenberg-Richter in a particular region is estimating the maximum size of an earthquake that can be hosted by the local faults. The largest earthquake in the Salton Sea Geothermal field region during the study period was an M5.1 and the neighboring, highly strained San Andreas fault can have earthquakes of magnitude at least 8.

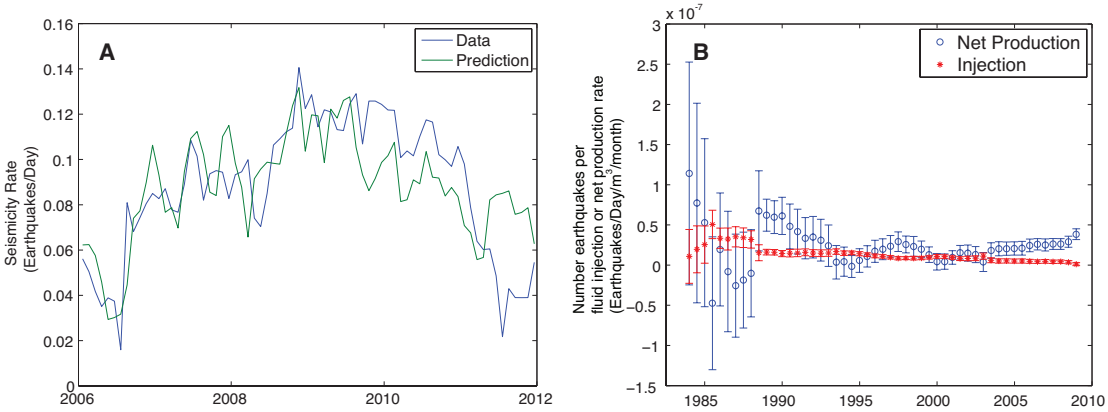

Figure 3. Results of linear model of seismicity based on a combination of injection and net production. (A) Sample seismicity rate and model prediction of seismicity rate using the observed fluid data and the best-fit linear model of Eq. 2. **(B)** Number of earthquakes per day triggered per rate of net volume of fluid extracted or total fluid injection. Symbols are best-fit coefficients for Eq. 2. The "Injection" values are coefficient c_1 in Eq. 2 and "Net Production" values are c_2. Error bars are 2 standard deviations of model estimates based on the linear regression.

Exemplary Figure

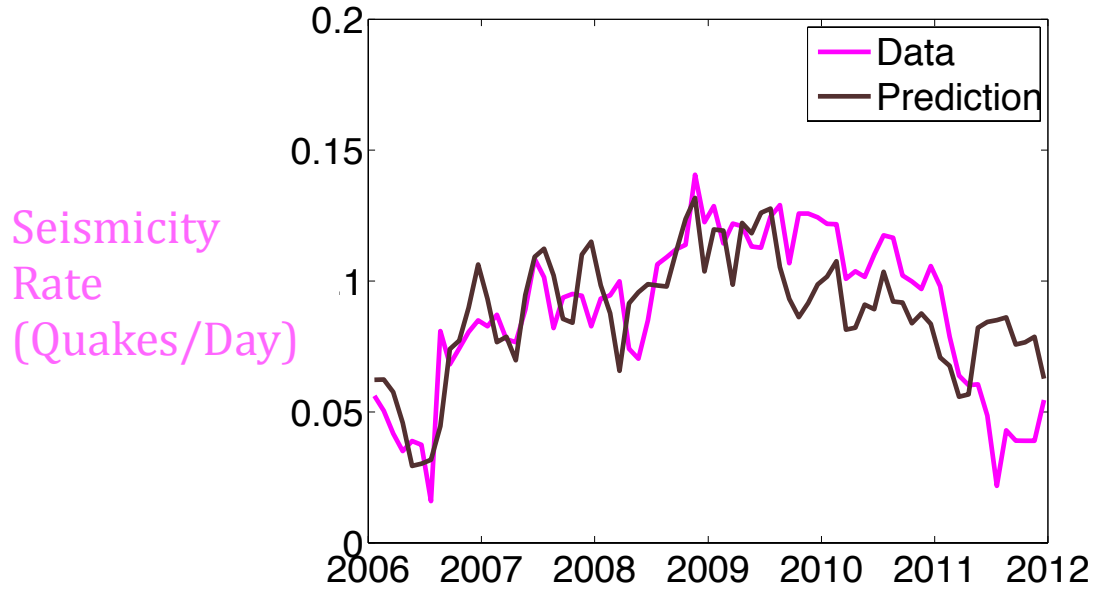

Results of linear model of seismicity based on a combination of injection and net production. Observed seismicity rate and model prediction of seismicity rate using the observed fluid data and the best-fit linear model.

INTELLECTUAL MERITS

The intellecutal merits of this work is in developing fundamental observations of earthquake rates in response to known stressing. In particular, fluid pressures are often evoked as a mechanism for triggering earthquakes, yet direct observations of the phenomenon under controlled conditions are limited. In addition, establishing that induced earthquakes have similar aftershock behavior to ordinary earthquakes constrains the mechanisms for interactions between faults.

BROADER IMPACT

Human-impacted earthquakes are a large and growing concern for society. Empirical methods, like that developed in this work, are desperately needed in order to guide policy.

REFERENCES AND NOTES:

Bachmann CE, Wiemer S, Woessner J, Hainzl S. 2011. Statistical analysis of the induced Basel 2006 earthquake sequence: introducing a probability-based monitoring approach for Enhanced Geothermal Systems. Geophysical Journal International **186** : 793–807. DOI: 10.1111/j.1365-246X.2011.05068.x

Brodsky EE. 2011. The spatial density of foreshocks. Geophysical Research Letters **38** DOI: 10.1029/2011GL047253

Chen X, Shearer PM. 2011. Comprehensive analysis of earthquake source spectra and swarms in the

Salton Trough, California. Journal of Geophysical Research **116** DOI: 10.1029/2011JB008263

Chu R, Helmberger DV. 2013. Source Parameters of the Shallow 2012 Brawley Earthquake, Imperial Valley. Bulletin Of The Seismological Society Of America **103** : 1141–1147. DOI: 10.1785/0120120324

Evans KF, Zappone A, Kraft T, Deichmann N, Moia F. 2012. Geothermics. Geothermics **41** : 30–54. DOI: 10.1016/j.geothermics.2011.08.002

Frohlich C, Hayward C, Stump B, Potter E. 2011. The Dallas-Fort Worth Earthquake Sequence: October 2008 through May 2009. Bulletin Of The Seismological Society Of America **101** : 327–340. DOI: 10.1785/0120100131

Hainzl S, Ogata Y. 2005. Detecting fluid signals in seismicity data through statistical earthquake modeling. Journal of Geophysical Research **110** : B05S07. DOI: 10.1029/2004JB003247 [online] Available from: http://www.agu.org/pubs/crossref/2005/2004JB003247.shtml

Hauksson E, Yang W, Shearer PM. 2012. Waveform Relocated Earthquake Catalog for Southern California (1981 to June 2011). Bulletin Of The Seismological Society Of America **102** : 2239–2244. DOI: 10.1785/0120120010

Keranen KM, Savage HM, Abers GA, Cochran ES. 2013. Potentially induced earthquakes in Oklahoma, USA: Links between wastewater injection and the 2011 Mw 5.7 earthquake sequence. Geology **41** : 699–702.

King G, Stein RS, Lin J. 1994. Static Stress Changes and the Triggering of Earthquakes. Bulletin Of The Seismological Society Of America **84** : 935–953.

Lei X, Yu G, Ma S, Wen X, Wang Q. 2008. Earthquakes induced by water injection at ~3 km depth within the Rongchang gas field, Chongqing, China. Journal of Geophysical Research **113** : B10310. DOI: 10.1029/2008JB005604

Llenos A, McGuire J, Ogata Y. 2009. Modeling seismic swarms triggered by aseismic transients. Earth and Planetary Science Letters **281** : 59–69.

Lohman RB, McGuire JJ. 2007. Earthquake swarms driven by aseismic creep in the Salton Trough, California. Journal of Geophysical Research **112** : 4405. DOI: 10.1029/2006JB004596

Majer E, Baria R, Stark M, Oates S, Bommer J, Smith B, Asanuma H. 2007. Induced seismicity associated with enhanced geothermal systems. Geothermics **36** : 185–222.

McGarr A, Simpson D, Seeber L. 2002. 40 Case histories of induced and triggered seismicity. In International Handbook of Earthquake and Engineering Seismology . Academic Press; 647–661.

Mossop A, Segall P. 1999. Volume strain within The Geysers geothermal field. Journal of Geophysical Research **104** : 29113–29131. DOI: 10.1029/1999JB900284

Muffler L, White DE. 1969. Active Metamorphism of Upper Cenozoic Sediments in the Salton Sea Geothermal Field and the Salton Trough, Southeastern California. Geological Society of America Bulletin **80** : 157–182.

Nicholson C, Wesson RL. 1992. Triggered earthquakes and deep well activities. Pure And Applied

Geophysics **139** : 561–578.

Nicol A, Carne R, Gerstenberger M, Christophersen A. 2011. Induced seismicity and its implications for CO2 storage risk. Energy Procedia **4** : 3699–3706. DOI: 10.1016/j.egypro.2011.02.302

Ogata Y. 1992. Detection of precursory relative quiescence before great earthquakes through a statistical model. Journal of Geophysical Research **97** : 19845–19871.

Raleigh CB, Healy JH, Bredehoeft JD. 1976. Experiment in Earthquake Control at Rangely, Colorado. Science **191** : 1230–1237.

Shapiro S, Dinske C, Langenbruch C, Wenzel F. 2010. Seismogenic index and magnitude probability of earthquakes induced during reservoir fluid stimulations. The Leading Edge **29** : 304.

van der Elst N, Brodsky EE. 2010. Connecting near-field and far-field earthquake triggering to dynamic strain. Journal of Geophysical Research **115** : B07311. DOI: 10.1029/2009JB006681

Woessner J, Hainzl S, Marzocchi W, Werner MJ, Lombardi AM, Catalli F, Enescu B, Cocco M, Gerstenberger MC, Wiemer S. 2011. A retrospective comparative forecast test on the 1992 Landers sequence. Journal of Geophysical Research **116** : 5305. DOI: 10.1029/2010JB007846

Younker LW, Kasameyer PW, Tewhey JD. 1982. Geological, geophysical, and thermal characteristics of the Salton Sea Geothermal Field, California. Journal Of Volcanology And Geothermal Research **12** : 221–258. DOI: 10.1016/0377-0273(82)90028-2

Presentations

Brodsky, E.E. and L.J. Lajoie ,V11D-07. Connecting Anthropogenic Seismicity Rates To Operational Parameters At The Salton Sea Geothermal Field, Southern California (Invited), Fall AGU 2013.

Lia J. Lajoie, Daniel R. O'Connell, Robert J. Creed and Emily E. Brodsky, S31F-01, Seismic response to power production at the Coso Geothermal field, south-eastern CA: using operational parameters and relocated events to study anthropogenic seismicity rates and reservoir scale tectonic structure, Fall AGU 2013.

Brodsky, E.E. and L.J. Lajoie ,V11D-07. Anthropogenic Seismicity Rates and Operational Parameters At The Salton Sea Geothermal Field, Annual SCEC meeting 2013.

Brodsky, E.E., Two Earthquake Problems with Industry Significance, MIT Earth Resources Lab, February 2014.

Brodsky, E.E. Induced Sesmicity: What do we need to know to be useful? Consortium on Environmental Consequences of Shale Gas, Calgary, Canada, April 2014.

Publications

Brodsky, E. E. and L.J. Lajoie, Connecting anthropogenic seismicity rates to operational parameters at the Salton Sea Geothermal Field, *Science*, DOI:10.1126/science.1239213.